Articles

Correlation between Protein Flexibility and Electron Transfer from $Q_A^{-\bullet}$ to Q_B in PSII Membrane Fragments from Spinach†

Axel Garbers,‡ Frank Reifarth,§ Jens Kurreck,§ Gernot Renger,§ and Fritz Parak*,‡

Physik Department E17, Technische Universität München, 85747 Garching, Germany, and Max-Volmer-Institut für Physikalische Chemie und Biochemie, Technische Universität Berlin, Strasse des 17. Juni 135, 10623 Berlin, Germany

Received February 5, 1998; Revised Manuscript Received June 11, 1998

ABSTRACT: To analyze a possible correlation between the extent of $Q_A^{-\bullet}$ reoxidation and protein dynamics, fluorometric and Mössbauer spectroscopic measurements were performed in photosystem II membrane fragments from spinach. Numerical evaluation of the flash-induced change of the normalized fluorescence quantum yield revealed that the extent of reoxidation starts to decrease below 275 K and is almost completely suppressed at 230 K. Detailed analyses of Mössbauer spectra measured at different temperatures in ^{57}Fe-enriched material indicate that the onset of fluctuations between conformational substates of the protein matrix occurs also at around 230 K. Based on this correspondence, protein flexibility is inferred to play a key role for $Q_A^{-\bullet}$ reoxidation in photosystem II. Taking into account the striking similarities with purple bacteria and the latest structural information on these reaction centers [Stowell, M. H. B., McPhillips, T. M., Rees, D. C., Soltis, S. M., Abresch, E., and Feher, G. (1997) *Science* **276**, 812−816], it appears most plausible that also the headgroup of plastoquinone-9 bound to the Q_B-site in PSII requires a structural reorientation for its reduction to the semiquinone.

The essential steps of photosynthetic water cleavage take place within a multimeric complex referred to as photosystem II (PSII)[1] that is anisotropically incorporated into the thylakoid membrane. PSII acts as a light-driven water plastoquinone oxidoreductase which gives rise to formation of molecular dioxygen released into the atmosphere and bound hydrogen in the form of plastoquinol (PQH_2). The latter reaction comprises a sequence of two univalent electron-transfer steps at a special protein pocket designated as the Q_B-site where a transiently attached plastoquinone-9 molecule becomes reduced by the one-electron donor $Q_A^{-\bullet}$. Component Q_A is a plastoquinone-9 molecule that is fixed by comparatively tight noncovalent binding and becomes reduced to its semiquinone form $Q_A^{-\bullet}$ as a result of the indispensable stabilization of primary charge separation [for a recent review, see (*1*)]. The first electron transfer from $Q_A^{-\bullet}$ to Q_B leads to a semiquinone ($Q_B^{-\bullet}$) which exhibits a high affinity to its binding site. After reduction by a second step and concomitant protonation from the stroma side, PQH_2 is formed and subsequently exchanged by another oxidized PQ molecule from the pool. The functional organization of this process closely resembles that of ubiquinol formation in anoxygenic purple bacteria [for a review, see (*2*)]. Likewise, the structural features are inferred to exhibit striking similarities (*3*, *4*). This idea is supported by recent findings indicating that the pattern of hydrogen bonding of $Q_A^{-\bullet}$ in PSII resembles that of purple bacteria (*5*).

There exist several lines of evidence that the electron-transfer steps from $Q_A^{-\bullet}$ to Q_B ($Q_B^{-\bullet}$) require structural flexibility of the protein matrix. This process was found to exhibit a striking temperature dependence. It becomes blocked at lower temperatures in both purple bacteria (*6*) and PSII (*7*). Analyses of the temperature dependence of $Q_A^{-\bullet}$ reoxidation led to the conclusion that the transition of PSII centers from inactive into active state for electron transfer is an entropy-driven process with a significant increase of 370 J K^{-1} mol^{-1} and 240 J K^{-1} mol^{-1} in thylakoids and PSII membrane fragments, respectively (*8*). Direct proof for the idea of electron transfer coupled to protein dynamics was recently presented by X-ray crystallography of reaction centers from the purple bacterium *Rhodobacter sphaeroides*. It was found that the head $Q_B^{-\bullet}$ is displaced by about 5 Å from the position of Q_B and the headgroup had rotated by 180° around the isoprene chain (*9*). Analogous studies on PSII cannot be performed so far because crystals of suitable diffraction properties are lacking. Therefore, another approach has to be used. Mössbauer spectroscopy has been proved to provide a powerful tool to study the flexibility of iron-containing proteins [for a review, see (*10*)]. The inner core of PSII contains two types of iron centers, the heme group(s) of cytochrome *b*559 (cyt *b*559) and the non-heme iron located between Q_A and Q_B. The latter type of iron is

† This work was supported by the Deutsche Forschungsgemeinschaft (Pa 178/14-3, Re 354/11-3) and the Fonds der Chemie.

* Corresponding author.
‡ Technische Universität München.
§ Technische Universität Berlin.

[1] Abbreviations: PSII, photosystem II; PQH_2, plastoquinol; NHE, non heme iron; cyt *b*559, cytochrome *b*559; hs, high spin; ls, low spin.

S0006-2960(98)00296-7 CCC: $15.00
Published on Web 07/31/1998

assumed to be coordinated by four histidines in an analogous manner as the corresponding non-heme iron in reation centers of purple bacteria (*3*, *4*), but the glutamate is replaced by bicarbonate acting as bidendate ligand (*11*). This difference in coordination might be responsible for the markedly lower redox potential of the NHE couple Fe^{3+}/Fe^{2+} in PSII (*12*−*14*). Mössbauer spectroscopy was successfully applied to unravel structure−function relations of the acceptor side of purple bacteria. It revealed a striking dependence of $Q_A^{-\bullet}$ reoxidation on protein flexibility (*6*). Analogous measurements in PSII preparations were performed only recently. In a short report, the reoxidation of $Q_A^{-\bullet}$ was shown to "freeze out" in a temperature region where the mobility of the iron becomes markedly restricted (*15*). The present report is a detailed study which shows that in PSII similar structure−function relations exist for $Q_A^{-\bullet}$ reoxidation as in purple bacteria.

MATERIALS AND METHODS

PSII membrane fragments were isolated from spinach according to the procedure described in (*16*) with slight modifications according to (*17*). After the final isolation step, the PSII membrane fragments were resuspended in 10 mM MES/NaOH (pH 6.5), 15 mM NaCl, 4 mM $MgCl_2$, 400 mM sucrose to chlorophyll concentrations of about 5 mg/mL. The samples were frozen in small aliquots in liquid nitrogen and stored at −80 °C until use.

Flash-induced changes of the fluorescence quantum yield were monitored with home-built equipment (*18*).

For Mössbauer spectroscopy, the samples were isolated from spinach grown hydroponically in a ^{57}Fe-enriched medium. The ^{57}Fe-PSII membrane fragments were concentrated by centrifugation at 165000*g*. Mössbauer experiments were performed at 155 K in a weak magnetic field perpendicular to the γ-beam using a ^{57}CoRh source as described in (*10*). All spectra were fitted by Lorentzians. The isomer shifts are given relative to metallic Fe as a reference.

RESULTS AND DISCUSSION

To analyze the correlation between electron transfer from $Q_A^{-\bullet}$ to Q_B and the protein dynamics, comparative measurements were performed on the temperature dependence of both properties.

Q_A^- Reoxidation as a Function of Temperature. The extent of $Q_A^{-\bullet}$ reoxidation was determined by measuring the transient flash-induced change of the normalized fluorescence quantum yield, $F_{var}^{norm}(t)$, as outlined in previous studies [see (*19*) and references cited therein]. Taking into account the nonlinear relationship between $F_{var}^{norm}(t)$ and the normalized population of $[Q_B^{-\bullet}(t)]$ (*20*), the latter parameter can be calculated by assuming reasonable values for the parameters that describe the excitation energy transfer between different photosynthetic units (*21*). Typical traces of $[Q_B^{-\bullet}(t)]$ gathered from $F_{var}^{norm}(t)$ at three different temperatures are shown in Figure 1.

At room temperature, the time course $[Q_A(t)]$ can be described by a triexponential decay and an offset that does not relax within a time domain of 10 s after the actinic flash (*8*, *19*):

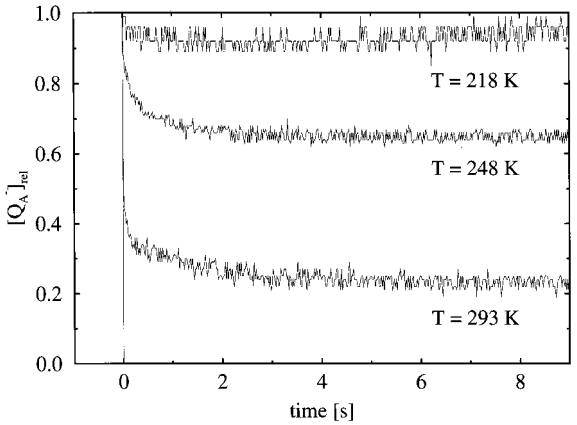

FIGURE 1: Normalized Q_A^- concentration as a function of time in dark-adapted PSII membrane fragments at different temperatures. For experimental details, see Materials and Methods.

$$[Q_A^{-\bullet}(t)] = [Q_A^{-\bullet}(t=0)]\sum_{i=1}^{3} a_i \exp(-t/\tau_i) + a_4 \quad (1)$$

The decay kinetics are ascribed to $Q_A^{-\bullet}$ reoxidation by (i) $Q_B(Q_B^-)$ in PSII complexes with a Q_B-site which is occupied by a PQ-9 molecule when $Q_A^{-\bullet}$ is formed (a_1, τ_1), (ii) a PQ-9 molecule of the pool which diffuses to an empty Q_B-site (a_2, τ_2), and (iii) recombination reactions with the donor side (a_3, τ_3).

In PSII membrane fragments with an intact water-oxidizing complex (WOC) $P680^{+\bullet}$ becomes rapidly reduced by tyrosine Y_Z followed by electron transfer from the WOC to Y_Z [for a review, see (*22*)]. Therefore, a back-reaction between $Q_A^{-\bullet}$ and either $P680^{+\bullet}$ or Y_Z^{OX} is negligibly small when the electron transport to the Q_B-site is intact. If this reaction is blocked (e.g., by DCMU), $Q_A^{-\bullet}$ becomes reoxidized by the WOC in redox state S_2 or S_3. Typical lifetimes are of the order of a few seconds at room temperature and 2 min at 258 K (*23*). If one takes into account that the donor side reactions leading to S_2 formation are not thermally blocked at T ≥ 200 K (*24*), the donor side can be ignored for interpretation of $Q_A^{-\bullet}$ reoxidation within a 10 s time domain. The small fraction of less than 10% found for a_3 is ascribed to PSII complexes which are not fully intact. This minor contribution will be neglected because it is not relevant for the topic of this study. Therefore, the normalized extent of a_4 reflects the fraction of $Q_A^{-\bullet}$ which remains oxidized due to incomplete electron transfer to PQ-9 in the Q_B-site. At room temperature, this phenomenon can be consistently explained by an equilibrium $Q_A^{-\bullet}Q_B/Q_B^{-\bullet}Q_A$ with a constant K_{eg} of the order of 10 corresponding with a Gibbs energy gap of 50−80 meV between states $Q_B^{-\bullet}/Q_B$ and $Q_A^{-\bullet}/Q_A$ (*2*, *25*).

The value of a_4 was found to increase drastically in thylakoids and PSII membrane fragments at lower temperatures. It approaches a value of close to 1 at 200 K; i.e., the electron resides at $Q_A^{-\bullet}$ in all PSII complexes within a time domain of 10 s after the actinic flash. This finding has been interpreted by the assumption that the energy gap becomes much larger (increase by ≥100 meV) due to structural constraints exerted by the protein matrix. Based on this idea, a most simple model has been proposed which includes only two states: an "active conformation" that

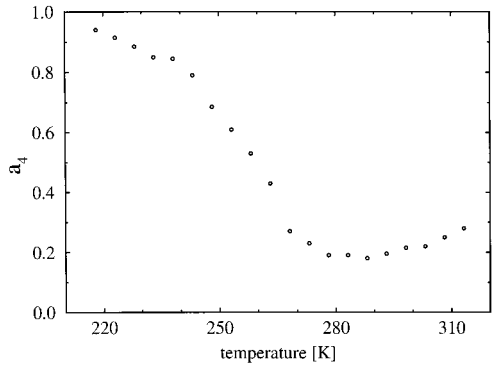

FIGURE 2: Temperature dependence of the amplitude a_4 of the nonrelaxing component of Q_A^- reoxidation in dark-adapted PSII membrane fragments. For details see text.

permits $Q_A^{-\bullet}$ reoxidation by Q_B and an "inactive conformation" where this process is blocked (*8*). This basic idea on the role of protein dynamics in electron transfer from $Q_A^{-\bullet}$ to Q_B is supported by theoretical calculations for the reaction centers of purple bacteria (*26*). The increase of a_4 can be interpreted to reflect a "freezing out" of the mobility of Q_B that is indispensable for its capability to accept electrons from $Q_A^{-\bullet}$. For the sake of direct comparability, the a_4 values were determined as a function temperature for the ^{57}Fe-labeled PSII membrane fragments used in this study for measurements of Mössbauer spectra. The results are depicted in Figure 2. They are in perfect agreement with previous findings (*8*). Of special relevance for the topic of this study is the steep decrease of a_4 in a comparatively narrow region between 230 and 260 K.

Protein Flexibility as a Function of Temperature. Figure 3 shows the Mössbauer spectrum of ^{57}Fe-labeled PSII membrane fragments measured at 155 K together with spectra at 200 K and 250 K. The deconvolution into one asymmetrical and two symmetrical quadrupole doublets with values for the isomer shifts and quadrupole splitting and their assignment to different iron centers compiled in Table 1 agree with previous reports in the literature (*15*, *27*). As the samples contain a heterogeneous cyt *b*559 population with a high- and a low-potential form [for a recent review, see (*28*)], the heme iron attains two different redox states at ambient potentials of the buffer, i.e., Fe(II) and Fe(III) which are both in the low-spin configuration. Accordingly, two doublets are due to cyt *b*559. The third doublet originates from the non-heme iron center that exhibits hyperfine parameters typical for a high-spin Fe(II) (*29*). Earlier studies revealed that the non-heme iron is found in two different microenvironments at $T = 80$ K (*30*). At temperatures above 100 K, this difference could not be resolved, and therefore the Lorentzian doublet gathered from deconvolution of the Mössbauer spectra represents the average values of both types of non-heme iron centers.

For an analysis of the protein dynamics, the Lamb Mössbauer factor, *f*, has to be extracted from the area, *A*, of the Mössbauer spectrum for each temperature. For the iron species *i*, the mean square displacement, $\langle x_i^2(T)\rangle$, can be obtained from

$$A_i = cf_i(T) = c\exp(-4\pi^2\langle x_i^2(T)\rangle/\lambda^2) \qquad (2)$$

where λ equals 0.86 Å for the 14.4 keV γ radiation of ^{57}Fe and *c* is a constant. The index *i* refers to the different iron species.

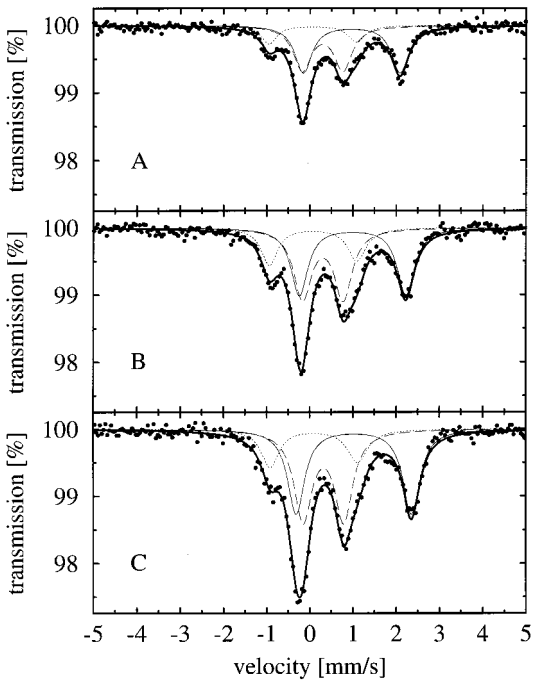

FIGURE 3: Representative Mössbauer spectra of ^{57}Fe-enriched PSII membrane fragments at 250 K (A), 200 K (B), and 155 K (C). Closed circles: experimental values. The thin-lined curves show the contributions of three quadrupole doublets simulated by Lorentzians. The associated iron species are NHE Fe(II)hs (solid curve), cyt *b*559 Fe(II)ls (dashed curve), and Fe(III)ls (dotted curve). The heavy-lined curve is the superposition of these components.

Table 1: Mössbauer Parameters of the Iron Centers Obtained from a Least-Squares Fit of Lorentzians to the Absorption Spectra of PSII Membrane Fragments at 155 K[a]

	isomer shift		quadrupole splitting	
type of iron center	155 K value (mm/s)	slope (mm/s K^{-1})	155 K value (mm/s)	slope (mm/s K^{-1})
cyt *b*559 Fe(II) low spin	0.44	-2.8×10^{-4}	0.94	$< -2 \times 10^{-5}$
cyt *b*559 Fe(III) low spin	0.21	-3.4×10^{-4}	2.03	$< -1 \times 10^{-5}$
NHE Fe(II) high spin	1.14	-5.9×10^{-4}	2.67	-4.5×10^{-3}

[a] The temperature dependence is obtained from the spectra in the temperature range of 120−250 K by smoothing procedures described in the text.

The constant *c* can be obtained by taking into account the fact that in many proteins the $\langle x^2\rangle$ values depend linearly on temperature between 180 K and about 20 K. Absolute mean square displacements are gathered from a linear extrapolation and the classical condition $\langle x^2\rangle = 0$ for $T = 0$ K.

The hyperfine parameters of the Mössbauer spectra at different temperatures were obtained by a least-squares fit. The results are summarized in Table 1 for one temperature. A comparison of the Mössbauer parameters at different temperatures (not shown) reveals that the quadrupole splitting of the non-heme high-spin iron, NHFe(II)hs, exhibit a marked decrease with increasing temperature, while those of the low-spin heme iron species, HFe(II)ls and HFe(III)ls, remain constant within the limits of statistical errors. The corresponding isomer shifts were found to decrease weakly toward higher temperatures. In a second step, an averaging of the

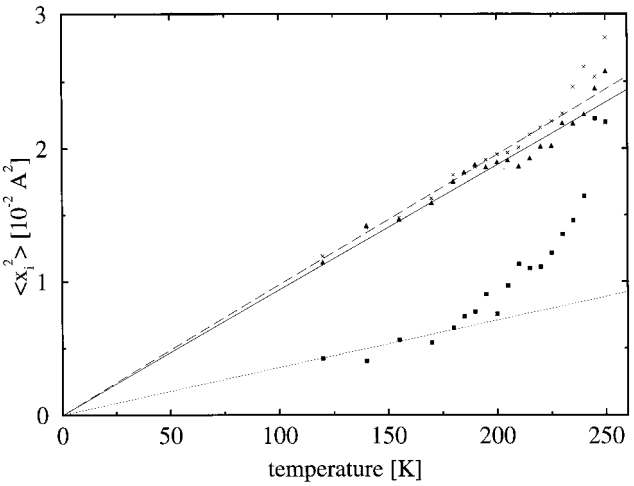

FIGURE 4: Mean square displacements of the different iron centers (symbols) in PSII membrane fragments. The contributions due to solid-state vibrations are marked through lines. Closed triangles and solid line, NHE Fe(II)hs; crosses and dashed line, cyt *b*559 Fe(II)ls; closed squares and dotted line, cyt *b*559 Fe (III)ls.

isomer shifts and the quadrupole splittings was performed, allowing a linear temperature dependence (slope in Table 1). With respect to the line width, different procedures were used for Fe(II) and Fe(III) species. For the ferrous iron species, the fluctuations of the line widths are smoothed by averaging the values of the fitted Lorentzians in the range of 120−200 K. Values above 200 K were not used because the statistical error of the data was too large. To obtain an optimal accuracy for the $\langle x_i^2(T)\rangle$ values, all Mössbauer spectra were refitted with the smoothed parameters allowing only a variation of the absorption areas A_i. In the case of ferric iron, the data analysis is more complicate. The rising magnetic hyperfine splitting due to a decrease in temperature has to be taken into account by broadened lines within the Lorentzian approximation. Therefore, the experimental line width of Fe(III)ls is given by

$$\Gamma_{exp} = 2\Gamma_{nat} + \Gamma_{inh} + \Gamma_{rel} \qquad (3)$$

where Γ_{nat} is the natural line width of the ^{57}Fe Mössbauer transitions and the factor 2 counts for the source and the absorber; Γ_{rel} reflects the contribution caused by relaxation, while Γ_{inh} accounts for the inhomogeneous environment of the Fe(III) within the proteins.

Based on the above-mentioned data analysis, the Lamb−Mössbauer factors of each iron species can be determined and the mean displacement calculated by using eq 1. The $\langle x_i^2(T)\rangle$ values obtained are shown in Figure 4 as a function of temperature. Two characteristic features emerge from this plot: (i) below a characteristic temperature, T_c, all three iron species exhibit a linear dependence of the mean square displacements on T; i.e., below T_c the slope of $\Delta\langle x_i^2(T)\rangle\Delta T$ is constant while it undergoes a pronounced increase above T_c; and (ii) for the low-potential cyt 599 species, HFe(III)ls, the value of the constant slope $\Delta\langle x_i^2(T)\rangle\Delta T$ is much smaller below T_c than the corresponding values for the high-potential cyt *b*559. HFe(II)ls and the NHFe(II)ls show almost the same slope.

With respect to the protein dynamics, the drastic increase of $\langle x_i^2(T)\rangle$ at a characteristic temperature T_c is the most interesting feature for a possible correlation between protein flexibility and electron transport. Earlier investigations have shown that in proteins bound to membrane fragments free diffusion processes can be ignored and, therefore, $\langle x_i^2(T)\rangle$ is described by a sum of two contributions (*31*, *32*):

$$\langle x_i^2(T)\rangle = \langle x_{i,v}^2(T)\rangle + \langle x_{i,t}^2(T)\rangle \qquad (4)$$

$\langle x_{i,v}^2(T)\rangle$ represents solid-state vibrations, and $\langle x_{i,t}^2(T)\rangle$ accounts for the fluctuations between conformational substates of the protein often called protein specific dynamics [for a review, we refer to (*33*)].

Recently it was shown that $\langle x_v^2(T)\rangle$ can be essentially explained by a normal-mode analysis in the case of myoglobin (*34*). The contributions of $\langle x_v^2(T)\rangle$ due to the three different iron species in PSII membrane fragments are represented by solid, dotted, and dashed lines in Figure 4. The fluctuation between conformational substates giving rise to $\langle x_{i,t}^2(T)\rangle$ are "frozen out" at low temperatures, and, therefore, this additional contribution to $\langle x_i^2\rangle$ occurs only above a certain threshold temperature. These fluctuations can be understood by a quasi-diffusive motion of segments of the protein molecule around the average position.

In several proteins, the characteristic temperature, T_c, for a drastic nonlinear increase is at about 180 K (*29*, *31*). An inspection of the results of Figure 4 reveals that the low-spin Fe(III) species might behave similar while the onset of the increased spatial fluctuations of both Fe(II) species occurs at markedly higher T_c values of about 230 K.

Evaluation of the Mössbauer spectra and optical measurements revealed that the PSII membrane fragments contain almost two cyt *b*559 per PSII [(*31*); see also (*28*)] with about 50% in the high- and low-potential forms, respectively. Accordingly, under our experimental conditions, cyt *b*559 attains both the Fe(II) and Fe(III) forms in a ratio close to 1:1. Recently it was shown that one of the heme groups is probably bound to an α_2 and the other one to a β_2 homodimeric protein matrix with the former located at the stroma and the latter at the lumen side (*36*).

It is, therefore, conceivable that the protein dynamics could be different for these two forms. An attractive possibility is the idea that both types of cyt *b*559 differ in their redox potential and the site of location. The Fe(II)ls of the high-potential form could be located near the acceptor side, and in this way both Fe(II) species are expected to exhibit similar protein dynamics as deduced from Figure 4. Further experiments are required to clarify this point. Regardless of this particular problem, the above-mentioned consideration clearly indicates that the protein dynamics of the non-heme iron species of PSII undergo a significant change at around 230 K.

Based on the above-mentioned considerations, straightforward conclusions can be obtained when the values $\langle x_i^2\rangle$ are derived from the sum of the areas of Mössbauer spectra belonging to the two Fe(II) species. The temperature dependence of these $\langle x_i^2\rangle$ values is depicted in Figure 5. For the sake of direct comparison, also the data of Figure 2 are redrawn that describe the temperature dependence of $Q_A^{-\bullet}$ reoxidation. The virtually identical onset of a drastic increase in both curves above 230 K provides convincing evidence for a correlation between protein dynamics and the electron transfer from $Q_A^{-\bullet}$ to Q_B in PSII. Protein fluctuations are

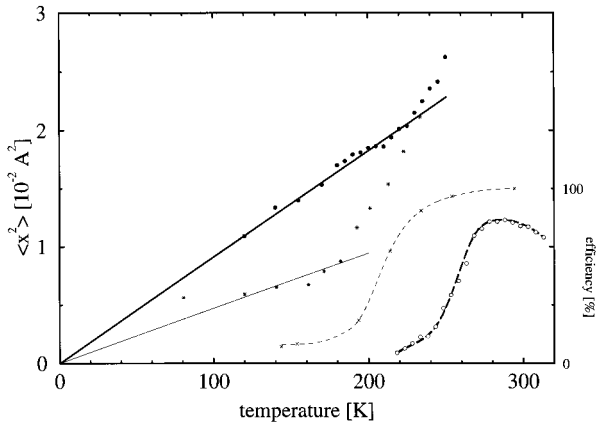

FIGURE 5: Mean square displacements obtained from the ferrous absorption areas of PSII membrane fragments (closed circles) and contribution originated by solid-state vibrations (thick solid line). The onset of protein-specific dynamics correlates to the increase in the efficiency of electron transfer from Q_A^- to $Q_B(Q_B^-)$ (open circles). The corresponding results found in chromatophore membranes from the purple bacterium *Rhodospirillum rubrum* (Parak, 1980) are added in the figure (stars, thin solid line, and crosses, respectively). Dashed lines are interpolations.

the lubricating grease for structural changes. This was also demonstrated in the case of myoglobin. Here, structural relaxation from the ligated to the unligated conformation [compare, e.g., (*37*)] becomes efficient only at temperatures above T_c, where protein-specific fluctuations are activated (*38*).

The idea of an intimate coupling between protein flexibility and $Q_A^{-\bullet}$ reoxidation by Q_B gains strong support by a comparison with corresponding data from purple bacteria where a drastic reorientation of the quinone headgroup in state $Q_B^{-\bullet}$ was observed by X-ray crystallography (*9*).

The corresponding data for the temperature dependence of $Q_A^{-\bullet}$ reoxidation and protein fluctuations, $\langle x_i^2(T)\rangle$, in the purple bacterium *Rhodospirillum rubrum* reported in a previous study (*6*) are redrawn in Figure 5. In this case, qualitatively the same correlation is observed between the onset of the electron transfer reaction and $\langle x_t^2(T)\rangle$. This phenomenon, together with the distinctly different constant slopes $\Delta\langle x_i^2(T)\rangle/\Delta T$ below T_c, suggests that the solid state properties of the matrix markedly differ in purple bacteria and PSII. An independent line of evidence for this idea is provided by the recent finding that a replacement of exchangeable protons by deuterons gives rise to different kinetic isotope effects on the electron transfer from $BPheo^{-\bullet}$ to Q_A in both types of organisms (*39*).

CONCLUDING REMARKS

The present study provides direct experimental evidence for a close correlation between $Q_A^{-\bullet}$ reoxidation by Q_B and protein dynamics. Based on the striking similarity with analogous features in purple bacteria, it is inferred that $Q_B^{-\bullet}$ formation in PSII requires a high flexibility of the PQ-9 molecule bound to the Q_B-site. It is attractive to speculate that the headgroup of PQ-9 associated with the Q_B-site undergoes a similar spatial displacement upon reduction to $Q_B^{-\bullet}$ as recently unraveled in purple bacteria (*9*). The idea is highly supported by recent findings indicating that in samples where state $Q_B^{-\bullet}$ is populated before freezing the $Q_A^{-\bullet}$ reoxidation can take place at much lower temperatures than in dark-adapted PSII membrane fragments (*40*). Despite similarities in the basic principles, it is also expected that quantitative differences exist because neither the functional redox group (ubiquinone versus plastoquinone) nor the structure of the Q_B-site are identical in purple bacteria and PSII. These differences are reflected by a gap of about 50 K in the threshold temperatures.

REFERENCES

1. Renger, G. (1992) in *Topics in Photosynthesis, The Photosystems: Structure, Function and Molecular Biology* (Barber, J., Ed.) pp 45−99, Elsevier, Amsterdam.
2. Crofts, A. R., and Wraight, C. A. (1983) *Biochim. Biophys. Acta 726*, 149−185.
3. Trebst, A. (1986) *Z. Naturforsch. 41C*, 240−245.
4. Michel, H., and Deisenhofer, J. (1988) *Biochemistry 27*, 1−7.
5. MacMillan, F., Lendzian, F., Renger, G., and Lubitz, W. (1995) *Biochemistry 34*, 8144−8156.
6. Parak, F., Frolov, E. N., Kononenko, A. A., Mössbauer, R. L., Goldanskii, V. I., and Rubin, A. B. (1980) *FEBS Lett. 117*, 368−372.
7. Joliot, P., and Joliot, A. (1973) *Biochim. Biophys. Acta 305*, 302−316.
8. Renger, G., Gleiter, H. M., Haag, E., and Reifarth, F. (1993) *Z. Naturforsch. 48C*, 234−240.
9. Stowell, M. H. B., McPhillips, T. M., Rees, D. C., Soltis, S. M., Abresch, E., and Feher, G. (1997) *Science 276*, 812−816.
10. Parak, F., and Reinisch, L. (1986) *Methods Enzymol. 131*, 568−607.
11. Hienerwadel, R., and Berthomieu, C. (1995) *Biochemistry 34*, 16288−16297.
12. Bowes, J. M., Crofts, C. A., and Itoh, S. (1979) *Biochim. Biophys. Acta 547*, 320−335.
13. Petrouleas, V., and Diner, B. A. (1987) *Biochim. Biophys. Acta 895*, 107−125.
14. Renger, G., Wacker, U., and Völker, M. (1987) *Photosynth. Res. 13*, 167−184.
15. Garbers, A., Kurreck, J., Reifarth, F., Renger, G., and Parak, F. (1996) *Proc. Int. Conf. Appl. Mössbauer Effect* (Ortalli, I., Ed.) Vol. 50, pp 811−814, SIF Bologna.
16. Berthod, D. A., Babcock, G. T., and Yocum, C. A. (1981) *FEBS Lett. 134*, 231−234.
17. Völker, M., Ono, T., Inoue, Y., and Renger, G. (1985) *Biochim. Biophys. Acta 806*, 25−34.
18. Gleiter, H. M., Ohad, N., Hirschberg, J., Fromme, R., Renger, G., Koike, H., and Inoue, Y. (1990) *Z. Naturforsch. 45C*, 252−258.
19. Renger, G., Eckert, H.-J., Bergmann, A., Bernarding, J., Liu, B., Napiwotzki, A., Reifarth, F., and Eichler, H.-J. (1995) *Aust. Plant Physiol. 22*, 167−181.
20. Joliot, A., and Joliot, P. (1964) *C.R. Acad. Sci. 258*, 4622−4625.
21. Dohnt, G., and Renger, G. (1984) in *Advances in Photosynthesis Research* (Sybesma, C., Ed.) Vol. 1, pp 429−432, Martinus Nijhoff/Dr. W. Junk Publishers, Den Haag, The Netherlands.
22. Renger, G. (1997) *Physiol. Plant. 100*, 828−841.
23. Renger, G., and Inoue, Y. (1983) *Biochim. Biophys. Acta 725*, 146−154.
24. Koike, H., and Inoue, Y. (1987) in *Progress in Photosynthesis Research* (Biggins, J., Ed.) Vol. 1, pp 645−648, Martinus Nijhoff, Dordrecht, The Netherlands.
25. Lavergne, J., and Briantais, J.-M. (1996) in *Advances in Photosynthesis* (Yocum, C. A., and Ort, D. R., Eds.) Vol. 4, pp 265−287, Kluwer Academic Press, Dordrecht, The Netherlands.
26. Beroza, P., Fredkin, D. R., Okamura, M. Y., and Feher, G. (1995) *Biophys. J. 68*, 2233−2250.
27. Petrouleas, V., and Diner, B. A. (1982) *FEBS Lett. 147* (1), 111−114.

28. Whitmarsh, J., and Pakrasi, H. B. (1996) in *Oxygenic Photosynthesis: The Light* Reactions (Ort, R., and Yocum, C. F., Eds.) pp 249−264, Kluwer, Dordrecht, The Netherlands.
29. Frolov, E., Birk, A., Fritzsch, G., Sinning, I., Michel, H., Goldanskii, V. I., and Parak, F. (1991) *Hyperfine Interact. 68*, 59−70.
30. Petrouleas, V., Sanakis, Y., Deligiannakis, Y., and Diner, B. A. (1992) in *Research in Photosynthesis* (Murata, N., Ed.) Vol. II, pp 119−122, Kluwer Academic Publishers, Dordrecht, The Netherlands.
31. Parak, F., Frolov, E. N., Mössbauer, R. L., and Goldanskii, V. I. (1981) *J. Mol. Biol. 145*, 825−833.
32. Parak, F., Knapp, E. W., and Kucheida, D. (1982) *J. Mol. Biol. 161*, 177−194.
33. Parak, F., and Frauenfelder, H. (1993) *Phys. Acta A201*, 332−345.
34. Melchers, B., Knapp, E. W., Parak, F., Cordone, L., Cupane, A., and Leone, M. (1996) *Biophys. J. 70*, 2092−2099.
35. Kurreck, J., Garbers, A., Reifarth, F., Andréasson, L.-E., Parak, F., and Renger, G. *FEBS Lett. 381*, 53−57.
36. McNamara, V. P., Suttervala, F., Pakrasi, H. B., and Whitmarsh, J. (1997) *Proc. Natl. Acad. Sci. U.S.A. 94*, 14173−14178.
37. Ansari, A., Berendzen, J., Bowne, S. F., Frauenfelder, H., Iben, I. E. T., Sauke, T. B., Shyamsunder, E., and Young, R. D. (1985) *Proc. Natl. Acad. Sci. U.S.A. 82*, 5000−5004.
38. Prusakov, V. E., Steyer, J., and Parak, F. G. (1995) *Biophys. J. 68*, 2524−2530.
39. Vasil′ev, S., Bergmann, A., Redlin, H., Eichler, H. J., and Renger, G. (1996) *Biochim. Biophys. Acta 1276*, 35−44.
40. Reifarth, F., and Renger, G. (1998) *FEBS Lett.* (in press).

BI980296+